CHEMICAL PHYSICS

Real-space analysis of diffusion behavior and activation energy of individual monatomic ions in a liquid

Tomohiro Miyata,[1]* Fumihiko Uesugi,[2] Teruyasu Mizoguchi[1]*

Investigation of the local dynamic behavior of atoms and molecules in liquids is crucial for revealing the origin of macroscopic liquid properties. Therefore, direct imaging of single atoms to understand their motions in liquids is desirable. Ionic liquids have been studied for various applications, in which they are used as electrolytes or solvents. However, atomic-scale diffusion and relaxation processes in ionic liquids have never been observed experimentally. We directly observe the motion of individual monatomic ions in an ionic liquid using scanning transmission electron microscopy (STEM) and reveal that the ions diffuse by a cage-jump mechanism. Moreover, we estimate the diffusion coefficient and activation energy for the diffusive jumps from the STEM images, which connect the atomic-scale dynamics to macroscopic liquid properties. Our method is the only available means to observe the motion, reactions, and energy barriers of atoms/molecules in liquids.

INTRODUCTION

Understanding atomic and molecular dynamics and reaction activities in liquids is crucial for developing higher-performance liquid systems because the macroscopic properties of a liquid, such as its viscosity and conductivity, are determined by the average local atomic and molecular dynamics and physical properties. However, gaining such an atomic- and molecular-scale understanding in liquids is highly challenging with conventional analytical methods, such as nuclear magnetic resonance and neutron scattering, which provide only averaged information on the whole liquid system. Thus, the development of a method for the high-resolution, real-space observation of the local dynamics and physical properties in liquids would provide important insight into the mechanisms that give rise to the macroscopic properties of liquids.

Among liquids, ionic liquids have unique properties, such as nonvolatility, high ionic density, and designable hydrophilicity (*1*–*3*). Owing to these properties, ionic liquids have been applied in a variety of industrial fields (for example, as electrolytes and extraction or reaction solvents) (*3*–*10*). Because ionic liquids exhibit unique diffusion behavior, which deviates strongly from the Stokes-Einstein behavior, it is necessary to gain an understanding of the dynamics of atoms and molecules within ionic liquids.

Here, we directly image individually dispersed monatomic ions in ionic liquids using atomic-resolution scanning transmission electron microscopy (STEM). To reveal the diffusion mechanism of monatomic ions, we analyze the dynamic motions of individual monatomic ions in an ionic liquid and furthermore, estimate local properties of the dynamics, such as diffusion coefficient and activation energy, by analyzing the STEM images.

RESULTS AND DISCUSSION

As schematically shown in Fig. 1, we observed gold (Au^{3+}) and iodide (I^-) dispersed in thin ionic liquid films using bright-field and annular dark-field (ADF) STEM. The simultaneously obtained bright-field and ADF images of the ionic liquid 1-ethyl-3-methylimidazolium bis(trifluoromethylsulfonyl)imide (C_2mimTFSI) with gold ions at room temperature are shown in Fig. 2 (A and B). The thickness of the observed area measured using the electron energy-loss spectroscopy log-ratio method is ~4 nm (*11*, *12*). Because the observation temperature (that is, room temperature) is higher than the melting point of C_2mimTFSI, it is considered to be in a liquid state. The shape of the liquid films substantially changes when the films remain tilted for several hours inside the TEM, as shown in fig. S1. Although the monatomic ions are not identifiable in the bright-field image, the ADF image shows numerous bright spots. We speculate them to be gold ions because gold has much higher atomic number (Z) in this composition and should be observed with much higher intensity as described in section S2. To confirm that the bright spots correspond to "single" gold ions, we compared the experimental bright-spot image with the simulated image, as shown in Fig. 2 (B and C). The intensity profiles of the experimental and simulated images are shown in Fig. 2D; there is good agreement between the experimental and simulated profiles. Furthermore, we constructed a

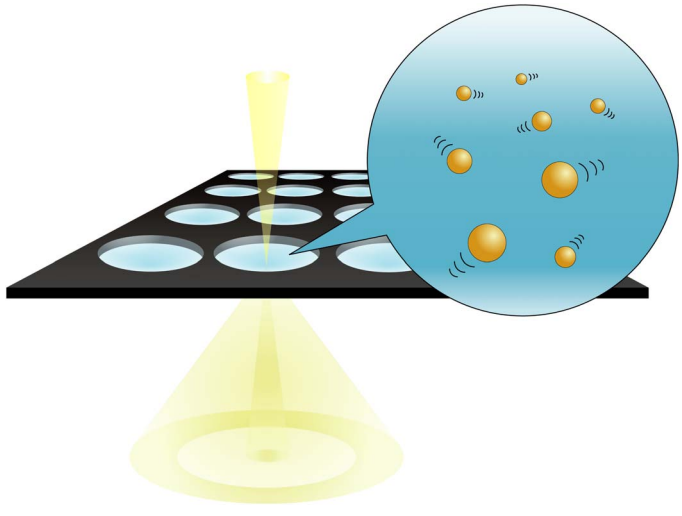

Fig. 1. Schematic representation of the observation method. Monatomic ion–dispersed ionic liquid forms ultrathin films in holes of a thin carbon film, and the electron beam is focused on the liquid film.

[1]Institute of Industrial Science, The University of Tokyo, 4-6-1 Komaba, Meguro, Tokyo 153-8505, Japan. [2]National Institute for Materials Science, 1-2-1 Sengen, Tsukuba, Ibaraki 305-0047, Japan.
*Corresponding author. Email: tomo-m@iis.u-tokyo.ac.jp (T.Miyata); teru@iis.u-tokyo.ac.jp (T.Mizoguchi)

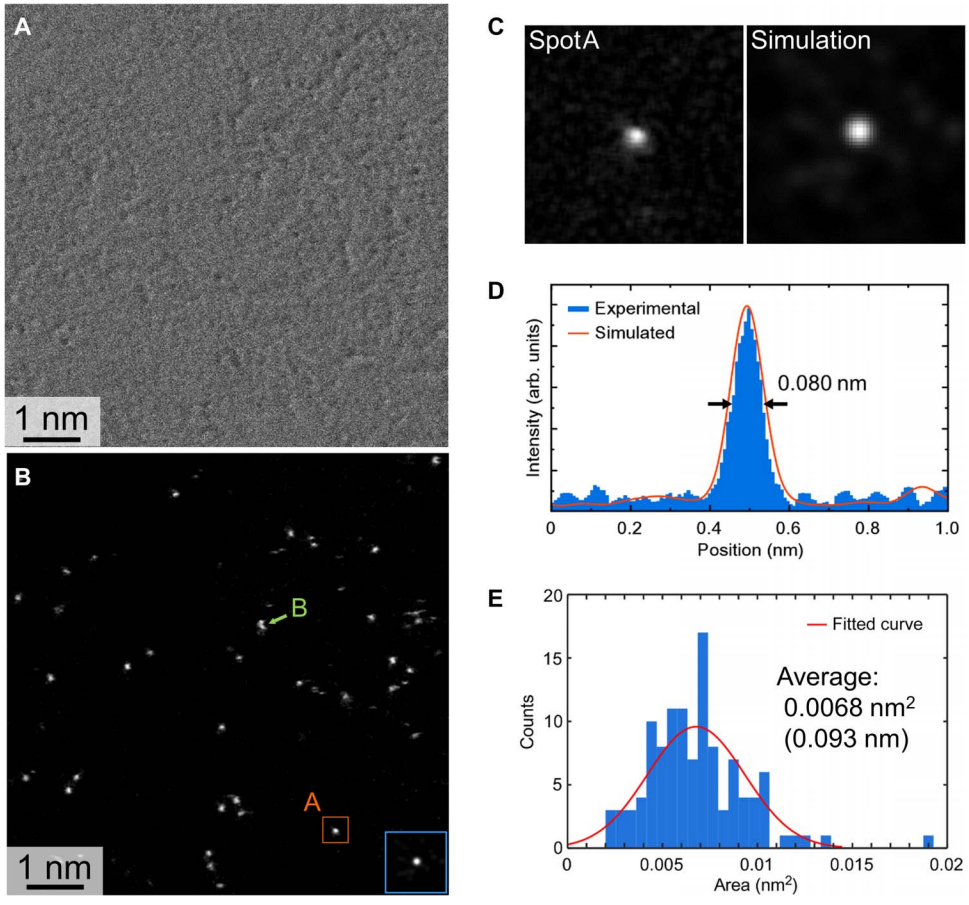

Fig. 2. Atomic-resolution imaging of monatomic gold ions in C_2mimTFSI. (**A** and **B**) Simultaneously obtained bright-field and ADF images. The inset at the bottom-right corner in (B) is the simulated image of a gold ion in C_2mimTFSI. (**C**) Left: Enlarged image of spot A and the simulated image in (B). (**D**) Intensity profiles of spot A and the simulated image in (C). arb. units, arbitrary units. (**E**) Histogram of the spot areas in (B).

histogram of the areas of the bright spots, as shown in Fig. 2E, which is fitted with a Gaussian curve, indicating an average value of 0.0068 nm^2. This area corresponds to a circle with a diameter of 0.093 nm, which is identical to the full width at half maximum of the simulated bright spot. On the basis of these results, we conclude that most of the bright spots in Fig. 2B correspond to single gold atoms. Thus, individual gold atoms (monatomic gold ions) in liquid C_2mimTFSI were directly observed using ADF STEM.

A more detailed inspection reveals that some bright spots have distorted shapes, owing to atomic vibrations or small displacements. As described in section S2, the absolute intensity of a monatomic gold ion without the background is independent of the liquid thickness, and the depth resolution is <9 nm. The 42 atoms in Fig. 2B correspond to a concentration of 0.29 M. This matches the atomic concentration of gold that was prepared and thus indicates that all the gold ions within the observation area are imaged. Moreover, we also performed atomic-resolution ADF observations of gold and iodine in different ionic liquids (section S1). These observations demonstrated that not only gold, but also iodine can be observed in ionic liquids.

Because individual gold ions in ionic liquids could be visualized, we investigated their dynamic behavior in C_2mimTFSI. First, we considered the atomic movement during the single-image observation in Fig. 2B. In this image, most of the bright spots have near-spherical shapes, and they are imaged within 15 scanning lines, which correspond to 0.114 nm (0.0076 nm per line). The acquisition time for a single, whole bright spot was approximately 0.25 s (section S3); that is, each of the ions is trapped in a very small space (or "cage"), which is accompanied by unidentifiable vibration for at least 0.25 s. It can be assumed that the monatomic gold ions are strongly solvated by the counterionic solvent molecules (*13*). By contrast, a few spots, such as spot B in Fig. 2B, show distinctly strained shapes, which are thought to originate from "jumping" from one cage to form a new cage or displacement accompanying the whole cage during imaging of the single gold ion. As shown in section S2, we simulated how a gold ion is imaged when it is displaced during imaging; a displacement >0.08 nm was found to be identifiable. In Fig. 2B, ~10% of the ions exhibit identifiable displacements. This behavior of the gold ions (that is, remaining in a cage and jumping from the cage) is supported by previously reported simulations of the diffusion of small ions in a similar ionic liquid (*13*).

Continuously acquired images of C_2mimTFSI with gold ions are shown in Fig. 3A. The liquid thickness is ~7 nm, and the frame rate is 4.2 s per frame. We confirmed that the damage caused by electron irradiation was not appreciable by imaging an area for several minutes (discussed in section S6). Labeled as A, B, and C in Fig. 3A, the ions were tracked, although spot B disappears in the image taken at 25.2 s as a result of jumping across the scanning line, and ion C appears to split into two spots (that is, C1 and C2) in the image taken at 29.4 s as a result of jumping from C1 to C2 during scanning.

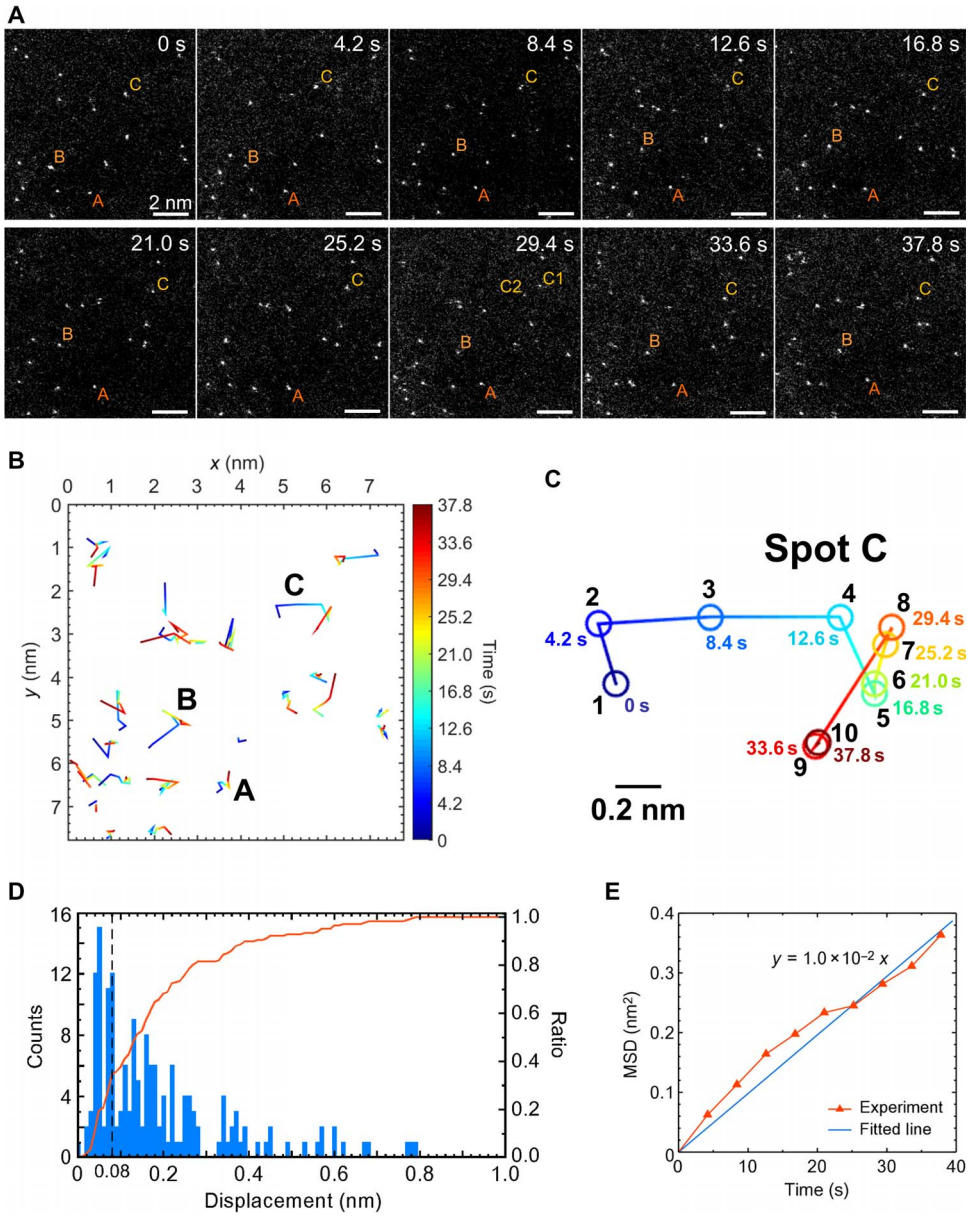

Fig. 3. Atomic diffusion analysis. (**A**) Continuous ADF images taken at a rate of 4.2 s per frame. The selected ions are labeled as A, B, and C. (**B**) Trajectory of the ions in (A). The labels A, B, and C are the same as those in (A). (**C**) Trajectory of spot C in (B). Each circled point is the position of ion C at the corresponding time. (**D**) Histogram of the atomic displacement within the duration of one frame. The left and right axes correspond to the number of ions and the integrated rate of the total number, respectively. (**E**) Mean square displacement (MSD) of the ions as a function of time.

The trajectories of all the ions are shown in Fig. 3B, in which it can be seen that the dynamics of the monatomic ions in the liquid phase are spatially and temporally heterogeneous in their displacement distances, directions, and times. As an example, we take the trajectory of ion C in Fig. 3C. The numbers in the figure correspond to the atomic positions in the respective frames. This trajectory shows that ion C often underwent large displacements within the 4.2-s scan (between frames 1 to 5, 6 and 7, and 8 and 9), as well as small jumps or displacements (between frames 5 and 6, 7 and 8, and 9 and 10). We consider this heterogeneity in the atomic dynamics to reflect the differences in the local solvation environment and temperature at each position. Small jumps or displacements (namely, between frames 5 and 6, 7 and 8, and 9 and 10) indicate that the monatomic gold ion was strongly caged by the surrounding solvent molecules or had low kinetic energy; by contrast, the ions moved under weakly constraining environments. We found that, contrary to the spatial and temporal heterogeneity, the displacements are completely isotropic on average as shown in section S4.

A histogram of the interframe displacements (within 4.2 s) of all ions is shown in Fig. 3D. The average displacement of the gold ions in the liquid is 0.19 nm per frame, and the number of gold ions remaining in the same positions (that is, displacement ≤ 0.08 nm) is 35%, indicating that 65% of the ions underwent several jumps or displacements within 4.2 s. In addition, most ions (94%) exhibit almost round shapes in all frames and thus remain in their original position for longer than 0.06 s (which is the scanning time of each round bright spot in these images). This result indicates that the transition of the relaxation behavior from

remaining in a cage to jumping between cages occurs on a time scale between 0.06 and 4.2 s in this system.

We then estimated the physical properties related to the diffusion of the monatomic gold ions in the liquid phase. The two-dimensional diffusion coefficient of the monatomic ions, $D_{2D,obs}$, was estimated to be 2.5×10^{-21} m^2 s^{-1} by measuring the mean square displacement (Fig. 3E). Furthermore, the activation energy for the diffusive jump of the monatomic ions was estimated using an approach with the diffusion coefficient, which gave a value of ~0.9 eV. This energy is reasonable, considering the small ionic size and high charge (*14*), and it leads to the slow motion of small ions. The details of the estimation method are described in section S5. Knowing these physical properties, such as the diffusion coefficient and the activation energy, enables a quantitative understanding of the atomic-scale local dynamics and environment, which determine the macroscopic properties.

In summary, we achieved direct imaging of monatomic gold ions in ionic liquids using STEM. Moreover, we observed the diffusion of the ions via a cage-jump mechanism, in which ions jump to form new cages. The diffusion behavior was spatially and temporally heterogeneous. Furthermore, the diffusion coefficient was estimated from the trajectory of the ions, and the activation energy for diffusion was estimated with an approach using the ionic diffusion coefficient.

Our observation and analysis method has the potential to reveal not only the diffusion and relaxation behavior of atoms and molecules, but also chemical reactions, such as atomic adsorption to and dissociation from catalytic molecules and nanoparticles, respectively, on the basis of the atomic-scale dynamics and activation energies. In addition, the liquid sample enables the investigation of liquid behavior in confined films by observing the dependence on the film thickness. We believe that our method will enhance the comprehensive understanding of phenomena occurring in liquids.

MATERIALS AND METHODS

Heavy-element ions were dispersed into the ionic liquids because they can be observed with *Z*-dependent contrast using ADF STEM (*15*, *16*).

Sample fabrication

We selected ionic liquid C_2mimTFSI (purity, 99.5%; Kanto Chemical Co. Inc.) as a solvent, the viscosity of which is 32 centipoise (at 298 K) (*17*). The vapor pressure at 298 K is approximately estimated to be 10^{-8} ~ 10^{-10} Pa (*18*). The melting point was measured to be −17.2°C by differential scanning calorimetry, which is consistent with previously reported values (*19*). Gold, a heavy element (Z_{Au} = 79), was dispersed into the solvent by blending with sodium tetrachloroaurate(III) dihydrate ($NaAuCl_4 \cdot 2H_2O$) (purity, 99.99%; Wako Pure Chemical Co.) at a concentration of ~0.1 M. Gold is present as Au^{3+} ions in these solutions. Liquid film samples for TEM observation were fabricated as follows (*11*, *20*). The ionic liquid solution was blended into ethanol at a ratio of 1:10. Next, ~2 μl of the solution was dropped onto a Quantifoil R1.2/1.3 holey carbon film (Quantifoil GmbH) with a thickness of ~40 to 50 nm (*11*); the ethanol was then evaporated by vacuum drying (~1 Pa, 100°C) for 20 min. The residual liquid, which is the heavy element–doped ionic liquid, forms thin films in the holes owing to surface tension.

STEM observations

We used an aberration-corrected STEM (JEM-ARM200CF, JEOL Ltd.) equipped with a cold-type field-emission gun operating at an accelerating voltage of 200 kV. The beam current was 9.5 pA (5.9×10^7 electrons s^{-1}) and the probe diameter was ~0.08 nm. The probe-forming aperture half-angle was 24.5 mrad; the detection angle was 0 to 9 mrad for bright-field imaging and 110 to 440 mrad for ADF imaging, which allows heavy atoms to be observed with high contrast to the background atoms (~Z^2). The imaging conditions for the experiments presented in Fig. 2 (A and B) were an image size of 1024 × 1024 pixels, a pixel size of 0.0076 nm per pixel, and a dwell time of 16 μs per pixel (the total acquisition time for one image was 16.8 s). The sequential images in Fig. 3A were observed with an image size of 512 × 512 pixels, a pixel size of 0.0152 nm per pixel, and a dwell time of 16 μs per pixel (acquisition time for one image of 4.2 s). Total dose for an image and dose rate per area were 2.5×10^8 electrons and 9.8×10^{23} electrons s^{-1} m^{-2}, respectively. The thickness of the observation area was measured by electron energy-loss spectroscopy using the log-ratio method (*12*). The image in Fig. 2B was processed by convoluting the averaging filter of 5 × 5 pixels with a value of 0.04. The room temperature was 23°C. The pressure in the STEM chamber was 2×10^{-5} Pa.

Molecular dynamics simulation

Molecular dynamics simulations were performed to construct liquid models for the ADF-STEM image simulation. In the C_2mimTFSI simulation, the charge of each atom was estimated via a first-principles numerical-basis molecular orbital calculation based on density-functional theory using the DMol^3 code for an isolated C_2mimTFSI molecule in a 1.5-nm cubic supercell. Next, 64 C_2mimTFSI molecules were set in a 3.015-nm cubic supercell (the density coincided with the experimental value of 1.518 g cm^{-3} at 25°C and 1 atm). A molecular dynamics simulation was then performed with the Forcite code under the conditions of the COMPASS II force field, an NVT ensemble, a time step of 1 fs, and a total time of 500 ps. The temperature was set to 1773 K to make an amorphous liquid structure in the short time.

Multislice image simulation

ADF image simulation was performed using the multislice method (*21*) with Dr. Probe high-resolution (S)TEM image simulation software. The C_2mimTFSI liquid structure with a thickness of 3 nm was prepared on the basis of the aforementioned structure determined by molecular dynamics simulations, and a gold atom was placed in the middle of the structure. The image was simulated from a 1-nm square of 64 × 64 pixels (0.0156 nm per pixel) centered on the gold atom, which satisfies the Nyquist sampling criterion. The image simulations were carried out under the same conditions as in the experiment. A Gaussian source profile with a full width at half maximum of 0.08 nm was convoluted on the simulated image. The frozen lattice model was applied to approximate the thermal atomic vibrations at each point.

Differential scanning calorimetry

Differential scanning calorimetry was performed using a DSC-60 Plus (Shimadzu Co.) instrument to know the melting point of the sample. The sample liquids were sealed in aluminum pans. The masses of the samples were 13 mg. The temperature range was −120 to 100°C, and the cooling and heating rate was set to 5°C min^{-1}.

SUPPLEMENTARY MATERIALS

Supplementary material for this article is available at http://advances.sciencemag.org/cgi/content/full/3/12/e1701546/DC1

section S1. ADF observation of different compositions (C_8mimCl-Au, C_2mimTFSI-I, and C_8mimCl-I)
section S2. Multislice image simulation for thickness, defocus, and composition dependence
section S3. Splitting spot analysis

REFERENCES AND NOTES

1. M. Armand, F. Endres, D. R. MacFarlane, H. Ohno, B. Scrosati, Ionic-liquid materials for the electrochemical challenges of the future. *Nat. Mater.* **8**, 621–629 (2009).
2. P. Wasserscheid, Chemistry: Volatile times for ionic liquids. *Nature* **439**, 797 (2006).
3. M.-C. Lin, M. Gong, B. Lu, Y. Wu, D.-Y. Wang, M. Guan, M. Angell, C. Chen, J. Yang, B.-J. Hwang, H. Dai, An ultrafast rechargeable aluminium-ion battery. *Nature* **520**, 324–328 (2015).
4. D. Larcher, J.-M. Tarascon, Towards greener and more sustainable batteries for electrical energy storage. *Nat. Chem.* **7**, 19–29 (2015).
5. X. Peng, H. Liu, Q. Yin, J. Wu, P. Chen, G. Zhang, G. Liu, C. Wu, Y. Xie, A zwitterionic gel electrolyte for efficient solid-state supercapacitors. *Nat. Commun.* **7**, 11782 (2016).
6. K. Prassides, Superconductivity: Interfaces heat up. *Nat. Mater.* **9**, 96–98 (2010).
7. Y. Saito, Y. Nakamura, M. S. Bahramy, Y. Kohama, J. Ye, Y. Kasahara, Y. Nakagawa, M. Onga, M. Tokunaga, T. Nojima, Y. Yanase, Y. Iwasa, Superconductivity protected by spin–valley locking in ion-gated MoS_2. *Nat. Phys.* **12**, 144–149 (2016).
8. B. A. Rosen, A. Salehi-Khojin, M. R. Thorson, W. Zhu, D. T. Whipple, P. J. A. Kenis, R. I. Masel, Ionic liquid–mediated selective conversion of CO_2 to CO at low overpotentials. *Science* **334**, 643–644 (2011).
9. M. Asadi, K. Kim, C. Liu, A. V. Addepalli, P. Abbasi, P. Yasaei, P. Phillips, A. Behranginia, J. M. Cerrato, R. Haasch, P. Zapol, B. Kumar, R. F. Klie, J. Abiade, L. A. Curtiss, A. Salehi-Khojin, Nanostructured transition metal dichalcogenide electrocatalysts for CO_2 reduction in ionic liquid. *Science* **353**, 467–470 (2016).
10. M. Matsumoto, Y. Saito, C. Park, T. Fukushima, T. Aida, Ultrahigh-throughput exfoliation of graphite into pristine 'single-layer' graphene using microwaves and molecularly engineered ionic liquids. *Nat. Chem.* **7**, 730–736 (2015).
11. T. Miyata, T. Mizoguchi, Fabrication of thin TEM sample of ionic liquid for high-resolution ELNES measurements. *Ultramicroscopy* **178**, 81–87 (2017).
12. T. Malis, S. C. Cheng, R. F. Egerton, EELS log-ratio technique for specimen-thickness measurement in the TEM. *J. Electron Microsc. Tech.* **8**, 193–200 (1988).
13. J. C. Araque, S. K. Yadav, M. Shadeck, M. Maroncelli, C. J. Margulis, How is diffusion of neutral and charged tracers related to the structure and dynamics of a room-temperature ionic liquid? Large deviations from Stokes-Einstein behavior explained. *J. Phys. Chem. B* **119**, 7015–7029 (2015).
14. M. Kofu, M. Tyagi, Y. Inamura, K. Miyazaki, O. Yamamuro, Quasielastic neutron scattering studies on glass-forming ionic liquids with imidazolium cations. *J. Chem. Phys.* **143**, 234502 (2015).
15. P. D. Nellist, S. J. Pennycook, Incoherent imaging using dynamically scattered coherent electrons. *Ultramicroscopy* **78**, 111–124 (1999).
16. T. Mizoguchi, S. D. Findlay, A. Masuno, Y. Saito, K. Yamaguchi, H. Inoue, Y. Ikuhara, Atomic-scale identification of individual lanthanide dopants in optical glass fiber. *ACS Nano* **7**, 5058–5063 (2013).
17. J. M. Crosthwaite, M. J. Muldoon, J. K. Dixon, J. L. Anderson, J. F. Brennecke, Phase transition and decomposition temperatures, heat capacities and viscosities of pyridinium ionic liquids. *J. Chem. Thermodyn.* **37**, 559–568 (2005).
18. D. H. Zaitsau, G. J. Kabo, A. A. Strechan, Y. U. Paulechka, A. Tschersich, S. P. Verevkin, A. Heintz, Experimental vapor pressures of 1-alkyl-3-methylimidazolium bis(trifluoromethylsulfonyl)imides and a correlation scheme for estimation of vaporization enthalpies of ionic liquids. *J. Phys. Chem. A* **110**, 7303–7306 (2006).
19. C. P. Fredlake, J. M. Crosthwaite, D. G. Hert, S. N. V. K. Aki, J. F. Brennecke, Thermophysical properties of imidazolium-based ionic liquids. *J. Chem. Eng. Data* **49**, 954–964 (2004).
20. T. Miyata, M. Fukuyama, A. Hibara, E. Okunishi, M. Mukai, T. Mizoguchi, Measurement of vibrational spectrum of liquid using monochromated scanning transmission electron microscopy–electron energy loss spectroscopy. *Microscopy* **63**, 377–382 (2014).
21. N. Calvar, E. Gómez, B. González, Á. Domínguez, Experimental determination, correlation, and prediction of physical properties of the ternary mixtures ethanol + water with 1-octyl-3-methylimidazolium chloride and 1-ethyl-3-methylimidazolium ethylsulfate. *J. Chem. Eng. Data* **52**, 2529–2535 (2007).
22. U. Domańska, E. Bogel-Łukasik, R. Bogel-Łukasik, 1-octanol/water partition coefficients of 1alkyl-3-methylimidazolium chloride. *Chem. Eur. J.* **9**, 3033–3041 (2003).
23. H. Zheng, S. A. Claridge, A. M. Minor, A. P. Alivisatos, U. Dahmen, Nanocrystal diffusion in a liquid thin film observed by in situ transmission electron microscopy. *Nano Lett.* **9**, 2460–2465 (2009).
24. J. M. Yuk, J. Park, P. Ercius, K. Kim, D. J. Hellebusch, M. F. Crommie, J. Y. Lee, A. Zettl, A. P. Alivisatos, High-resolution EM of colloidal nanocrystal growth using graphene liquid cells. *Science* **336**, 61–64 (2012).
25. E. R. White, M. Mecklenburg, B. Shevitski, S. B. Singer, B. C. Regan, Charged nanoparticle dynamics in water induced by scanning transmission electron microscopy. *Langmuir* **28**, 3695–3698 (2012).
26. A. Bondi, van der Waals volumes and radii. *J. Phys. Chem.* **68**, 441–451 (1964).
27. A. Noda, K. Hayamizu, M. Watanabe, Pulsed-gradient spin–echo ^{1}H and ^{19}F NMR ionic diffusion coefficient, viscosity, and ionic conductivity of non-chloroaluminate room-temperature ionic liquids. *J. Phys. Chem. B* **105**, 4603–4610 (2001).
28. A. Kaintz, G. Baker, A. Benesi, M. Maroncelli, Solute diffusion in ionic liquids, NMR measurements and comparisons to conventional solvents. *J. Phys. Chem. B* **117**, 11697–11708 (2013).
29. S.-H. Chong, F. Hirata, Dynamics of ions in liquid water: An interaction-site-model description. *J. Chem. Phys.* **111**, 3654–3667 (1999).
30. H. Matsubara, F. Pichierri, K. Kurihara, Mechanism of diffusion slowdown in confined liquids. *Phys. Rev. Lett.* **109**, 197801 (2012).
31. R. G. Evans, O. V. Klymenko, P. D. Price, S. G. Davies, C. Hardacre, R. G. Compton, A comparative electrochemical study of diffusion in room temperature ionic liquid solvents versus acetonitrile. *ChemPhysChem* **6**, 526–533 (2005).
32. R. D. Shannon, Revised effective ionic radii and systematic studies of interatomic distances in halides and chalcogenides. *Acta Crystallogr. Sect. A Found. Adv.* **A32**, 751–767 (1976).
33. J. T. Edward, Molecular volumes and the Stokes-Einstein equation. *J. Chem. Educ.* **47**, 261 (1970).
34. F. Castiglione, E. Ragg, A. Mele, G. B. Appetecchi, M. Montanino, S. Passerini, Molecular environment and enhanced diffusivity of Li^+ ions in lithium-salt-doped ionic liquid electrolytes. *J. Phys. Chem. Lett.* **2**, 153–157 (2011).
35. R. F. Egerton, P. Li, M. Malac, Radiation damage in the TEM and SEM. *Micron* **35**, 399–409 (2004).
36. R. F. Egerton, *Electron Energy-Loss Spectroscopy in the Electron Microscopy* (Springer, ed. 3, 2011).
37. W. M. Haynes, D. R. Lide, T. J. Bruno, *CRC Handbook of Chemistry and Physics, 96th Edition* (CRC Press, 2015).
38. M. Mizoshiri, T. Nagao, Y. Mizoguchi, M. Yao, Dielectric permittivity of room temperature ionic liquids: A relation to the polar and nonpolar domain structures. *J. Chem. Phys.* **132**, 164510 (2010).

Acknowledgments: The STEM measurements were conducted at the Research Hub for Advanced Nano Characterization, National Institute for Materials Science, under the support of "Nanotechnology Platform" (no. 12024046) of the Ministry of Education, Culture, Sports, Science and Technology (MEXT), Japan. T. Miyata would like to thank T. Kamoi and S. Kamoi for modifying the illustration in Fig. 1. **Funding:** This study was supported by the Mitsubishi Science Foundation (27143), Grants-in-Aid for Scientific Research from MEXT (nos. 25106003, 26630302, 26249092, and JP17H06094), a Grant-in-Aid from the Japan Society for the Promotion of Science Fellows (no. 15J11146), and Japan Science and Technology Agency (JST)–Precursory Research for Embryonic Science and Technology (PRESTO). **Author contributions:** T. Miyata performed the experiments and wrote the paper. F.U. provided support and advice for the experiments. T. Mizoguchi discussed the results and directed the entire study. All authors read and commented on the manuscript. **Competing interests:** The authors declare that they have no competing interests. **Data and materials availability:** All data needed to evaluate the conclusions in the paper are present in the paper and/or the Supplementary Materials. Additional data related to this paper may be requested from the authors.

Submitted 10 May 2017
Accepted 10 November 2017
Published 15 December 2017
10.1126/sciadv.1701546

Citation: T. Miyata, F. Uesugi, T. Mizoguchi, Real-space analysis of diffusion behavior and activation energy of individual monatomic ions in a liquid. *Sci. Adv.* **3**, e1701546 (2017).

Science Advances

Real-space analysis of diffusion behavior and activation energy of individual monatomic ions in a liquid

Tomohiro Miyata, Fumihiko Uesugi and Teruyasu Mizoguchi

Sci Adv **3** (12), e1701546.
DOI: 10.1126/sciadv.1701546